
NeuralODF: Learning Omnidirectional Distance Fields for 3D Shape Representation

Trevor Houchens*
Brown University
trevor_houchens@brown.edu

Cheng-You Lu*
Brown University
cheng-you_lu@brown.edu

Shivam Duggal
Carnegie Mellon University
sduggal@andrew.cmu.edu

Rao Fu
Brown University
rao_fu@brown.edu

Srinath Sridhar
Brown University
srinath@brown.edu

Abstract

In visual computing, 3D geometry is represented in many different forms including meshes, point clouds, voxel grids, level sets, and depth images. Each representation is suited for different tasks thus making the transformation of one representation into another (forward map) an important and common problem. We propose Omnidirectional Distance Fields (ODFs), a new 3D shape representation that encodes geometry by storing the depth to the object’s surface from any 3D position in any viewing direction. Since *rays* are the fundamental unit of an ODF, it can be used to easily transform to and from common 3D representations like meshes or point clouds. Different from level set methods that are limited to representing closed surfaces, ODFs are unsigned and can thus model open surfaces (*e.g.*, garments). We demonstrate that ODFs can be effectively learned with a neural network (NeuralODF) despite the inherent discontinuities at occlusion boundaries. We also introduce efficient forward mapping algorithms for transforming ODFs to and from common 3D representations. Specifically, we introduce an efficient Jumping Cubes algorithm for generating meshes from ODFs. Experiments demonstrate that NeuralODF can learn to capture high-quality shape by overfitting to a single object, and also learn to generalize on common shape categories.

1 Introduction

Representing the 3D shape of objects and scenes is a fundamental problem in visual computing. Shape representations such as point clouds, meshes, voxel grids, level sets, depth images and multi-view images are widely used in 3D scene reconstruction, rendering, design, or 3D printing. Each representation has its own advantages and issues for use in downstream tasks, so transforming one to another is an important task.

Recently, a class of coordinate-based neural networks, known as *neural fields* [52] or *neural implicit functions*, have been used to learn these 3D shape representations [38, 35, 21, 55, 9]. These *neural shape fields* parametrize 3D shape using coordinates in a bounded volume or a surface, and have been shown to be useful for shape modeling, and reconstructing shapes from images or other partial inputs. Existing neural shape fields are typically trained by sampling the underlying 3D representation they model (*e.g.*, SDFs). To produce suitable outputs for downstream tasks (*e.g.*, meshes), a **forward map** [52] is used. Common examples of forward maps include marching cubes [34] for extracting meshes from level sets, ray marching [40] for rendering (depth) images from level sets, and surface

* Authors contributed equally to this work.

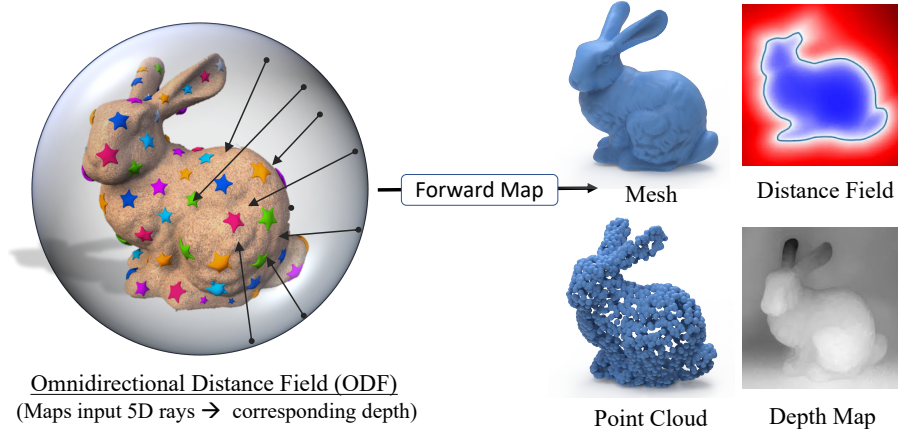


Figure 1: We introduce **Omnidirectional Distance Field (ODF)**, a new 3D shape representation that takes a 5D input, $\vec{r} = (x, \hat{w})$, specifying a ray originating at a 3D location x and oriented along a direction \hat{w} . For each such ray, an ODF outputs the depth to the surface of the 3D shape along the input ray. We show that **NeuralODF** can implicitly learn an ODF when trained on rays sampled within a region around the shape (sphere shown above). We also show that NeuralODF can be easily transformed to common shape representations like meshes, points clouds, or depth maps using computationally-efficient forward maps [52].

splatting [59] for rendering from point clouds. However, forward maps to transform neural shape fields to common representations can be complex and computationally expensive. Moreover, many extant neural shape fields [38, 35] can only model *watertight (closed) surfaces*—shapes with a clearly defined inside and outside—preventing their use in modeling open surface shapes like garments.

In this paper, we address these limitations by proposing **Omnidirectional Distance Field (ODF)**, a new 3D shape representation that allows more efficient forward mapping to common shape representations while capturing both open and watertight surfaces. An ODF implicitly encodes object geometry by storing the distance to the object’s surface from any 3D position, x , in any viewing direction, \hat{w} . For any open or closed surface $\partial\Omega$ we formally define an ODF as

$$d(x, \hat{w}) = \min(\|x - x_I\|_2), x_I \in \partial\Omega,$$

where $x_I = x + t \cdot \hat{w}$ with $t \geq 0$. **The fundamental building block of an ODF is a ray.** Intuitively, an ODF stores the depth of the rays cast towards a surface in any direction (omnidirectional) and originating at any 3D point (see Figure 1). ODFs generalize unsigned distance fields [10] to all directions, and can be used to represent open surfaces. However, an ODF is parametrized in 5D (3D position and 2D direction) making it inefficient for storage and high-resolution querying. Therefore, we show that a neural network, **NeuralODF**, can implicitly learn an ODF for efficient storage and fast querying. At inference, rather than estimate the ray depths in a single forward pass, we use a recursive approach to estimate higher-quality shapes. Since ODFs are inherently discontinuous at occlusion boundaries, NeuralODF also estimates visibility enabling it to handle these discontinuities.

The omnidirectional distance information in a NeuralODF enables us to build forward maps to extract meshes, depth images, point clouds, and voxel grids more efficiently than for existing neural shape fields (see Figure 1). To extract point clouds or depth maps from NeuralODF, the forward map is a trivial recursive forward pass of the network. To extract signed or unsigned distance fields, the forward map is a minimum operator over depth in all directions: $\min_{\forall i}[d(x, \hat{w}_i)]$. To extract occupancy voxel grids, the forward map is a minimum operator over the intersection mask in all directions. Finally, to extract meshes we propose a new forward map called **Jumping Cubes**, a more efficient variant of marching cubes that exploits the omnidirectional information and can handle open surfaces.

Experiments demonstrate that NeuralODF learns to overfit high-quality shapes for single shape instances, with both open and closed surfaces. NeuralODF also generalizes to a category of shapes when trained using an autoencoder framework [38]. Our method can also handle occlusion boundaries and surface frontiers. We envision NeuralODF to be used in applications that require learning from and producing different 3D representations. In summary, our contributions are:

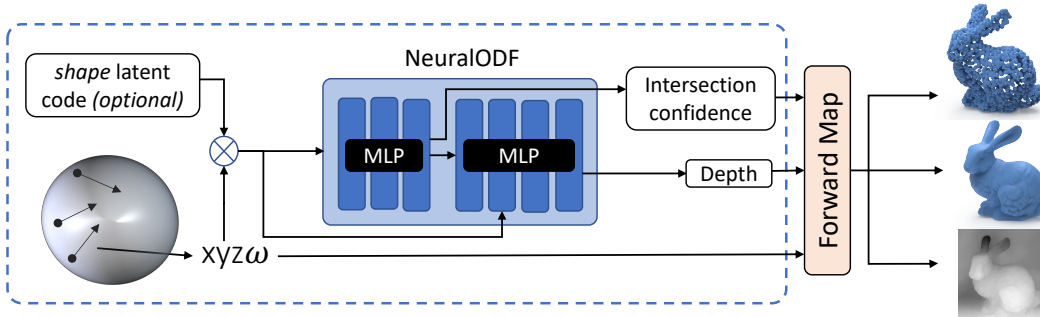


Figure 2: **Overview of NeuralODF:** The proposed neural omnidirectional distance field is trained using a set of sampled 5D rays (directed arrows in the sphere above), and the associated depth and intersection labels as output. For each sampled ray $\vec{r} = (x, \hat{w})$, the NeuralODF module predicts an intersection confidence and a depth-to-surface estimate. We use a recursive inference procedure for higher quality shape reconstruction, where we recursively query the NeuralODF at multiple points along the input ray to extract the final surface point. Once learned, we can map the learned ODF to 3D representations like meshes, point clouds, and depth maps. NeuralODF can be used for both overfitting a single shape and generalizing to a category of shapes.

- A novel 3D representation, **Omnidirectional Distance Fields (ODFs)**, that returns the distance to the surface for any ray in 3D space.
- **NeuralODF**, a method for learning ODFs using a recursive neural network.
- Forward mapping algorithms to efficiently extract common 3D representations like depth images, meshes (**Jumping Cubes**), and point clouds from ODFs/NeuralODFs.

2 Related Work

In this brief survey of related work, we focus on learning-based methods (including neural shape fields [52]) for 3D shape representations such as point clouds, voxels, meshes, parametric surfaces, level sets, multi-view images, and radiance fields.

Point Clouds: Point clouds are one of the most common 3D geometric data structures. Therefore, representing and processing point clouds with neural networks has been an important topic of recent work [41, 50, 42, 44]. Early work used features extracted from permutation-invariant networks like PointNet together with an adversarial loss [1, 31], while other methods use convolution-based architectures [16]. Another approach is to start with a regular point set, sampled either on a grid [55] or from a normal distribution [54], and then advected them to appropriate 3D locations to represent the shape. Point clouds can be transformed to other representations, but the process can be slow and inaccurate (*e.g.*, Poisson surface reconstruction [27]). Different from these methods, NeuralODF can trivially produce point cloud outputs (Section 4.2) that can be sampled at arbitrary resolutions in addition to producing other common representations.

Voxels: Voxels are another common 3D representation that are easy to store, query and manipulate. Some methods extend the notion of 2D convolution to 3D voxels [11, 33, 26]. Using neural nets to estimate voxel occupancy is a common approach, for instance, in Occupancy Networks [35]. Since capturing small-scale detail is difficult with a global latent code, some methods divide the shape into smaller latent code grids [39]. Voxel grids generally lack the ability to capture small details at lower resolutions, while storage and compute requirements for higher resolutions grow exponentially. They are also not conducive for transforming to other representations easily due to missing details.

Meshes / Parametric Surfaces: Meshes are perhaps the most common 3D data structure used widely in rendering and 3D reconstruction. Since meshes are irregular, graph/geodesic convolution operations are a common choice within neural networks [7, 56, 22, 55]. Features learned on mesh vertices can directly be learned for use in downstream tasks [23, 51, 48, 17, 13]. However, meshes have fixed topology and resolution, so some methods have focused on *parametric surfaces* that can be sampled at any resolution [21, 14, 29]. While these methods are continuous, they have difficulty reconstructing shapes with varying topology. Due to their popularity, well established methods exist for converting meshes to point clouds and depth images [40, 24].

Level Sets / Distance Fields: Level sets such as signed distance fields (SDFs) are suitable for representing shapes of varying topology. Multiple methods have demonstrated that SDFs can be learned with a neural network [38, 15], and can be further improved by regularizations (*e.g.*, Eikonal property) specific to SDFs [19]. Marching Cubes [34, 32] is a popular method for converting level sets to meshes. However, SDFs are constrained to modeling watertight shapes limiting their use in open surfaces (*e.g.*, garments). Unsigned distance fields [10] (with Ball-Pivoting [5]) and GIFS [58] are alternatives that support open surfaces and mesh generation. To model high-quality shape, recent methods employ vector quantization together with transformers [53, 37]. Concurrent to our work, Probabilistic Directed Distance Fields [2] were recently introduced and use a similar shape representation as us. However, their focus is on differentiable rendering, and the use of regularization for handling discontinuities. In contrast, we focus on efficient forward maps for shape reconstruction, and show that a recursive MLP is sufficient to learn ODFs thus reducing complexity.

Multi-View Images / Radiance Fields: While outside our scope, we note that ODFs are connected to networks that learn from multi-view images and are used to render photo-realistic novel views. Methods like NeRF [36], SRNs [46], VolSDF [57] and NeuS [49] implicitly encode the scene radiance / geometry and require ray marching to extract depth maps. Recently, Light Field Networks [45] accelerated the neural rendering process by directly parameterizing the radiance observed by each ray. Unlike Light Field Networks [45] which focuses on scene radiance, our focus is on accurate 3D shapes. Our method could be used to speed up rendering and efficiently extract depth maps.

3 ODF: Omnidirectional Distance Field

In this work, we propose a new 3D representation called Omnidirectional Distance Field (ODF) that is inspired by light fields [18, 30] for modeling the 5-dimensional plenoptic function [4, 28]. Similar to a light field, an ODF is also a 5D function that implicitly encodes 3D geometry by storing the depth to a shape’s surface along rays intersecting it. Formally, we define an ODF as a function $\text{ODF}(\vec{r}) = (d, p)$, which takes as input a vector defining the input ray $\vec{r} = (x, \hat{w})$, where x denotes the ray starting point and \hat{w} denotes a unit ray direction. For each input ray, the ODF function outputs a scalar depth value ($d \in \mathbb{R}^+$) to the surface of the underlying geometry (see Figure 3). Since some rays will never intersect the shape, an ODF additionally stores a binary flag ($p \in \{0, 1\}$) to indicate intersection. For ray \vec{r} intersecting the surface (*i.e.*, $p = 1$), the intersection point can be directly generated in $\mathcal{O}(1)$ complexity as: $x + \hat{w}d$.

ODFs store omnidirectional information at each 3D point and thus encode rich information about the geometry. This enables us to build more efficient forward mapping functions compared to other shape representations.

ODFs Generalize SDFs/UDFs: Signed/unsigned distance field (SDF/UDF) at a given point x refers to the shortest distance (along the surface normal) from the input point to the surface of the geometry. The sign of the SDF specifies whether the sampled point is inside or outside the geometry, whereas a UDF is unsigned. Compared to SDFs/UDFs, ODFs model the distance to the surface along **any given input direction**, thus an *SDF/UDF is a slice of the ODF along the surface normal direction*. In this paper, we focus on *unsigned* ODFs that encode a positive scalar distance for modeling open surfaces. However, signed ODFs can also be constructed.

Recursive Property: An accurate SDF satisfies the Eikonal property, which states that the magnitude of the gradient of the signed distance field should satisfy $\|\nabla \text{SDF}(x)\| = 1$. Recent works [20] leverage this property to regularize learned SDFs. Similarly, since an ODF is parameterized by the ray direction (\hat{w}), it also satisfies the property that the magnitude of the *directional derivative* of the ODF’s depth estimate should be equal to 1, *i.e.*, $\|\nabla_{\hat{w}} \text{ODF}_{\text{depth}}(x, \hat{w})\| = 1$. This property makes ODFs a recursive function of the depth value:

$$\|\text{ODF}_{\text{depth}}(x, \hat{w})\| = \|\text{ODF}_{\text{depth}}(x - \hat{w}, \hat{w})\| + 1$$

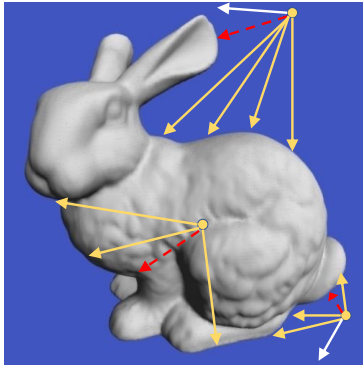


Figure 3: An ODF maps all input rays ($\vec{r} = (x, \hat{w})$) to the corresponding depths and intersections (white rays do not intersect, yellow rays intersect, red rays model SDF/UDF).

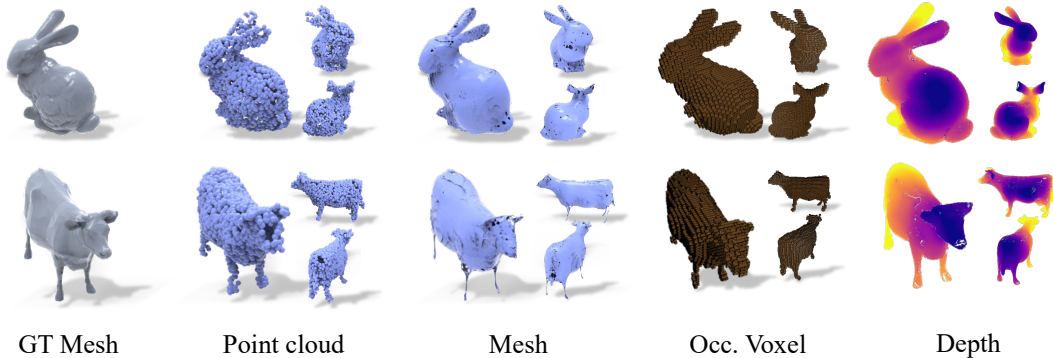


Figure 4: **Various 3D representations extracted from learned NeuralODF:** We showcase ODF’s 3D fitting capability through a mesh \rightarrow ODF \rightarrow {point cloud, mesh, voxel, depth} transformation.

We use this recursive property to regularize our learned ODFs via data augmentation (see Section 4.1).

4 NeuralODF: Neural Omnidirectional Distance Fields

While an ODF can be stored and queried without using neural networks, this can be computationally expensive due to dimensionality and result in low-quality shapes. To capture details and to enable sampling continuously at arbitrary resolutions [43], we build upon recent successes in neural shape fields that learn shape representations implicitly [38, 21, 36]. We first describe our procedure to learn NeuralODF, and then our forward mapping algorithms that use the NeuralODF to extract common 3D representations such as meshes, point clouds, and depth maps.

4.1 Constructing NeuralODF

To learn ODFs with a neural network, we adopt a supervised training strategy. Learning an ODF requires us to sample *rays* around 3D shapes, build a neural network that can learn to estimate the depth and intersection of these rays, and propose an inference procedure to sample the ODF at arbitrary resolutions. Furthermore, we would like to support overfitting of single shapes, as well as generalization to categories of shapes.

Sampling Rays for Learning: As described in Section 3, rays are the fundamental building block of an ODF. Thus, to learn an ODF, we first need to sample rays around shapes that we are interested in capturing. The input to NeuralODF could be any one of the common shape representations like meshes, depth maps, or point clouds. To generate training data from these input representations, we sample a set of 5D rays ($\vec{r} = (x, \hat{w})$) with associated depth and intersection mask. We use well-established techniques to sample rays from common representations, for instance, fast rendering for meshes, pixel sampling for depth maps, or ray sampling around point clouds. This allows us to obtain a balanced random sample of intersecting and non-intersecting rays distributed uniformly within an enclosed volume (sphere of radius = 1.3). We discuss the specific parameters in our data preparation procedure in Section 5.1. Our focus is on unsigned ODFs for modeling open surfaces, so we only use positive scalars for depth. Formally, each instance in our training data refers to a pair of ray starting point and unit direction: (x, \hat{w}) , together with labels that store the depth to the surface (d), and intersection (p). For rays not intersecting the 3D geometry, the depth value is set to 0.5. Our training rays are shown as directed arrows within a sphere in Figure 2.

Network Architecture: Inspired by previous work that learn high dimensional functions [36, 38], NeuralODF uses an MLP architecture (see Figure 2) to learn ODFs. It consists of eight feed-forward dense layers (with ReLU activation and Layernorm [3]). The input to this network is a ray denoted by 3D position and 2D orientation (5D). The output of this network is an intersection confidence value and a depth along the ray. We output the intersection confidence after two layers in order to *leave larger network capacity for the harder depth estimation task*. We also include a skip connection of the input 5D coordinates (and latent code) for better depth estimation.

Overfitting & Generalization: NeuralODF supports both overfitting a single shape or generalizing to a category of shapes. For overfitting (Section 6.1), we directly train NeuralODF on a given shape’s

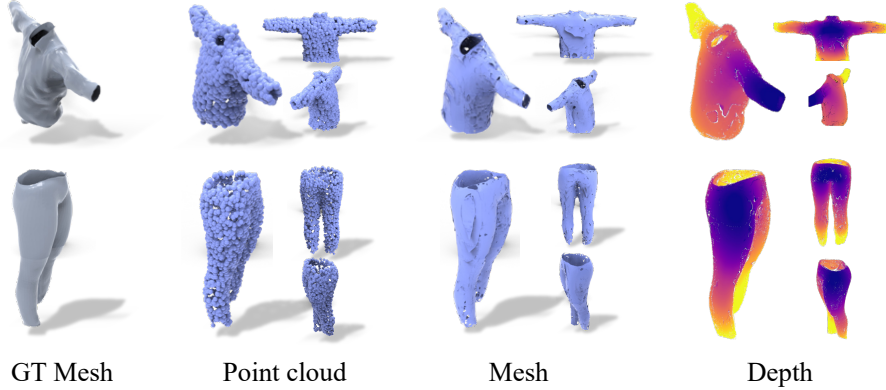


Figure 5: **Open surface extraction using NeuralODF:** Open-surface 3D garments reconstructed through a mesh \rightarrow ODF \rightarrow {point cloud, mesh, voxel, rendered depth maps} transformation.

training data (rays). To generalize to a category of shapes (Section 6.2), we adopt the autoencoder framework [38]. During training, we jointly optimize the network weights and a 256-dimensional latent code for each instance in the shape category. During inference, each latent code maps to a unique instance in the category and new latent codes can also be optimized for unseen instances.

Recursive Inference: During inference, a forward pass of NeuralODF can directly be used to obtain intersection and depth for any ray within the volume. However, this can often result in noisy estimates, especially for rays originating far from the surface. For higher shape quality, we introduce a recursive inference strategy that progressively refines the depth estimate along a given ray. For an input ray \vec{r} , we first estimate $\text{ODF}_{\text{depth}}(x, \hat{w})$ and obtain a new 3D location x_1 that is the putative surface. We then recurse inference from x_1 along the same direction \hat{w} until the estimated depth difference is small (empirically set to 3 iterations, see supplementary). This recursive procedure leads to higher quality shapes.

Loss Functions: The training of ODF is guided by two loss terms: mean square error (ℓ_{depth}) with the GT for the depth prediction and binary cross-entropy loss (ℓ_{prob}) for the intersection confidence prediction task. Like TSDFs [12, 38], we clamp both the predicted and ground truth depth to a max value of 0.5, to better utilize the network capacity for near-surface points. We follow [38] to regularize the latent code with ℓ_2 norm for generalization ($\ell_{\text{regularization}}$). The overall loss is:

$$\ell_{\text{all}} = \lambda_1 \ell_{\text{depth}} + \ell_{\text{prob}} + \lambda_2 * \ell_{\text{regularization}}$$

We set λ_1 to 5 and λ_2 to 0.0001 in our experiments.

4.2 Forward Mapping ODF to Common 3D Representations

Defining geometry as an ODF allows us to extract various 3D representations, such as meshes, point clouds, depth maps and implicit functions at reduced time complexities and memory due to the omnidirectional information. Once trained, we utilize the learned NeuralODF module to extract different shape representations at inference time as described below.

ODF to Depth Maps: By learning the underlying geometry in terms of ODF, the rendering procedure used to render the depth maps reduces to a constant $\mathcal{O}(1)$ complexity algorithm. Given an input camera viewpoint, we shoot multiple rays from the given camera center in different directions corresponding to the underlying pixel locations and camera intrinsics. A depth map can then be rendered by simply mapping the space of generated rays to the corresponding depth values obtained from the ODF. For better accuracy, we use 3 recursion steps in all our results.

ODF to Point Clouds: To extract a 3D point cloud from the ODF, we first sample 3D points within a sphere (radius=1.3 used in experiments) enclosing the underlying geometry. These 3D points serve as the ray starting points. For each ray starting point, we then uniformly sample a ray direction and (recursively) estimate the depth of a superset of rays (65K in our experiments). Some of these rays do not intersect and are discarded. Thus, the point cloud is simply the points corresponding to the depth of the intersecting rays.



Figure 6: **Generalization of NeuralODF to Shapenet chairs and planes**

ODF to Mesh: The forward map for extracting a mesh out of a signed distance field is typically the marching cubes algorithm [34]. Marching cubes involve using the SDF values for each point in a lattice and then leveraging those values to determine the location of mesh faces (a mesh face occurs whenever there is a sign change in the SDF values of the neighbouring lattice points). To generate a 3D mesh, the marching cubes algorithm performs a set of mesh intersection tests for each unit cube of the 3D lattice. However, unlike SDF, the ODF value at a point on the lattice determines the depth to the geometric surface from that point. This enables us to build a more efficient version of marching cubes that we call **Jumping Cubes**. Based on the predicted depth estimates, Jumping Cubes skips a series of neighbouring cubes. For instance, if depth to the surface along the x-direction from a lattice cube point is k , then it means that a mesh face would occur between the $\lfloor n + k \rfloor$ and $\lceil n + k \rceil$ lattice unit cubes and we can thus skip evaluating k unit cubes between n th and $\lfloor n + k \rfloor$ cube. Please see the supplementary document for details.

ODF to Others: ODFs can also be forward mapped to SDFs/UDFs since ODFs are a superset of these fields. At a given point x , we randomly sample N different directions (all intersecting, *i.e.*, $p = 1$). We can then find the SDF/UDF value at that location by $SDF(x) = \min_{\forall i} [ODF_{depth}(x, \hat{w}_i)]$. We also show examples of generating voxel grids/occupancy using ODFs (see Figure 4).

5 Experiment Details

5.1 Training Data Preparation

To validate the efficiency of the learned ODF, we perform two sets of experiments: *single-instance fitting experiments and generalization experiments*. In order to train the ODF for either of these experiments, we need to sample many ground-truth (GT) 5D rays, associated with the corresponding GT surface intersection probability and GT depth-to-surface estimates. While generating ground-truth SDF data requires a training instance to be a watertight 3D mesh [38], the training instances for extracting ODF data (5D rays with depth and intersection estimates) need not be water-tight and can be in either mesh, point cloud or depth map representation. All our experiments are categorized based on the input and the output representations used (*i.e.* input representation \rightarrow ODF \rightarrow output representation). We now define the strategies to map different input representations to ODF:

Multi-view depth maps to ODF: When training instances are available as a collection of 2.5D depth maps, the GT training ray data is simply the set of rays connecting the corresponding camera center to different depth-map pixel locations. We used depth maps of resolution 256×256 for our experiments. The camera centers for generating the depth maps are sampled on the surface of the enclosing sphere (radius = 1.3) and the camera’s principle axis direction connects the camera center to the enclosing sphere center.

Mesh to ODF: When training instances are available as 3D meshes, we use two strategies to generate the training data: (a) For 60% of the total sampled rays, we uniformly sample the ray starting point within the enclosing sphere and uniformly sample a ray direction from the surface of the unit sphere. (b) For 40% of the rays, we first uniformly sample ray end points on the surface of the mesh and then sample ray start points inside the enclosing sphere. The ray direction is then simply the normalized vector connecting start and end points. For both the strategies, after sampling the ray start points and the directions, we determine the depth to surface (and hence recompute the end points) by performing ray-mesh intersection queries (using trimesh).

Training data Augmentation: To further augment the training data, we leverage the recursive property of the ODF and perform the following augmentations: (a) Perturbation of the ray starting point along the chosen ray direction. (b) Perturbation of the ray end points along the chosen ray direction, and using them as the ray start points. The resulting ray direction in this case is opposite of the perturbation direction. The perturbations are restricted to be less than 0.1/0.01 for

Method	Depth Metrics		Intersection Conf. Metrics	
	CD↓	F-score (%)↑	Rec.(%)	F-score (%)
NeuralODF	0.302	24.91	96.29	94.65
UDF	0.857	15.80	86.94	80.77

Table 1: Avg. results on single-object fitting

Category	Depth Metrics		Intersection Conf.	
	CD↓	F-score (%)↑	Rec. (%)↑	F-score (%)↑
Airplane	0.976	13.82	96.82	86.47
Car	1.339	12.86	97.69	94.52
Chair	1.105	13.05	96.07	90.11

Table 2: Generalization of ODF on Shapenet

overfitting/generalization. (c) Using the original ray end-points (surface points for intersecting rays) as the reference points. The new ray directions and start points are then sampled uniformly, centered at the reference points. The magnitude of the rays is restricted by 0.1/0.01 for overfitting/generalization.

The last two augmentation strategies are used to sample 3D points near the surface of the input geometry. Please refer to supp. for ablation on these training data augmentation strategies.

5.2 Datasets

For the experiments involving fitting to a single 3D shape, we use the commonly used CAD models in graphics to generate the input data: Stanford bunny, XYZ-RGB Asian dragon, cow and armadillo from Alec Jacobson’s repository [25]. For demonstrating the efficiency of ODF in reconstructing open-surfaces, we also experiment on some garment instances [6].

For the generalization experiments, we train the proposed NeuralODF and the baselines on the Shapenet [8] cars, chairs and airplanes dataset. We leverage 1200 CAD models as training instances and 100 CAD models as test instances. Based on the input representation used for each experiment, we first map the CAD models to the corresponding input representation and then use the procedures mentioned in section 5.1 to map the input representation to the ODF training data.

5.3 Metrics

We evaluate both the intersecting probability and depth prediction of the generated ODFs.

Metrics for evaluating depth prediction: We compute the chamfer distance (scaled by 1000) between the GT point cloud and the predicted point cloud (generated as the ray end-points of the intersecting rays). Finally, a f-score metric with threshold 0.005 is provided.

Metrics for evaluating intersection probability prediction: For all input rays (intersecting and non-intersecting), we compare the GT and the predicted intersection probability through recall and f-score metrics. Please refer to supp. for more details on the metrics.

6 Experimental Results

6.1 Single-instance fitting experiments

In this section, we test the capability of ODFs to fit to a single 3D training instance. We take ground-truth 3D shape of a single training object in an arbitrary input representation (depth map or mesh) and then map the input 3D representation to the ODF training data (section 5.1). We then fit the NeuralODF module to the ODF data of the input 3D geometry. Once learned, we can then map the learned ODF to other 3D shape representations like meshes, point clouds, occupancy voxel grids and depth maps. In Figure 4, we train perform the experiment of mapping input mesh representation to ODF, which is then forward mapped to various different output representations (mesh \rightarrow ODF \rightarrow {mesh, point cloud, voxel, 2.5D depth map}). From Figure 4, we can see that the proposed NeuralODF module is able to reconstruct the *finer details* (*bunny ears, cow horns*) in the reconstructed shapes. The depth maps can be rendered in $\mathcal{O}(1)$ complexity, much faster than prior ray-marching based approaches [57, 36, 49, 47]. In Figure 5, we perform the same experiment for open-surface objects, which are difficult to model with signed-distance based approaches [38]. Thanks to the unsigned nature of the ODF, we are able to *model the open-surfaces well and maintain the topology of the GT shape*. Table 1 quantitatively validates NeuralODF’s performance.

6.2 Generalization experiments

NeuralODF is also able to generalize to unseen shapes. In this section, we train an autoencoder on 1200 ShapeNet objects [8] for each of the airplanes, cars, and chairs classes. At inference time, we

use 8 multi-view depth images from an unseen instance to optimize a new latent code. In Figure 6 we use these latent codes to reconstruct unseen objects in various output representations. We can see that NeuralODF is able to capture important details like chair legs and jet engines on new instances. Classes with holes, like slatted chair backs, appear to be more difficult. Table 2 assesses the performance of our autodecoder.

We also compare our method to Unsigned Distance Fields (UDF) on the task of shape generation. First, we compare with a UDF that utilizes our NeuralODF architecture without the intersection branch. It is trained in the same manner as the NeuralODF network, but the training data consists of the UDF values instead of ODF values, and there is no viewing direction. Both NeuralODF and this UDF are trained on the same 1200 instances of the ShapeNet chair dataset, and are then evaluated on a further 100 unseen instances. The metrics we use to compare these methods are the Chamfer- L_2 distance (scaled by 1000), and the F-Score with a threshold of 0.005 applied to point clouds (of equal size) extracted from each network. Table 3 shows the results of the ShapeNet chairs generalization task. Results of overfitting these methods on 8 instances can be seen in Table 1. Both experiments show that NeuralODF is able to better reconstruct point clouds than UDFs with a similar architecture and training regimen.

We also compare NeuralODF to Neural Unsigned Distance Fields [10] (referred to as NeuralUDF), a recent method for learning unsigned distance fields from point clouds. We compare our methods on the task of shape generalization on the ShapeNet cars dataset. Our NeuralODF is trained on a subset of their training data consisting of 917 car instances. Both models are evaluated on the same 77 unseen instances. We then sample a dense point cloud of 20,000 points from the surface of the ground truth mesh and compare it to the point cloud reconstructions from both methods to calculate the Chamfer- L_2 distance (scaled by 1000) and the F-score with a threshold of 0.005. Table 3 demonstrates that NeuralODF is competitive with NeuralUDF, although we are modeling a higher dimensional field.

Category	Method	Depth Metrics	
		CD ↓	F-score (%) ↑
Car	NeuralUDF	1.832	2.92
	NeuralODF (Ours)	1.904	2.18
Chair	UDF	1.457	12.21
	NeuralODF (Ours)	1.105	13.05

Table 3: Point cloud reconstruction comparison on Shapenet dataset

6.3 Ablation study

We perform several ablations to justify different choices made in the NeuralODF pipeline.

Ablation on recursive inference algorithm: Through Table 4 we ablate the recursive inference algorithm used to forward map ODFs to different 3D representations (section 4.2). From the table, we see that by *using the recursive inference algorithm, we can reduce the chamfer error of the reconstructed point cloud by 12.3% and increase the F-score of the predicted intersection confidence by 21.9% (row 1 vs row 2)*. On further increasing the number of recursion steps (from 3 to 5) for ray marching using ODF, we notice an increase in the chamfer value. This is potentially because of the noise in the learned ODF and our recursive logic which could lead to the network predicting to the network predicting surfaces behind the viewpoint after many iterations.

Iter.	Depth Metrics	Intersection Conf. Metrics	
	CD ↓	Rec. ↑ (%)	F-score (%) ↑
1	0.425	59.41	72.66
3	0.302	96.29	94.65
5	0.351	96.40	94.62

Table 4: Iterations of Recursive inference

Training Set	Depth Metrics	Intersection Conf. Metrics	
	CD ↓	Rec. (%) ↑	F-score (%) ↑
Mesh	0.302	96.29	94.65
Depth Images	1.621	92.87	88.60

Table 5: NeuralODF with various fidelity

Ablation of input representations used for learning ODF: As mentioned in Section 5.1, ODF can be learned from various input representations (meshes, depth maps). To demonstrate this utility, we compare the single instance fitting capability using ODF training data generated from GT multi-view (8 in experiments) depth maps vs the ODF training data generated from GT meshes. From the table 5, we can see that the point clouds reconstructed using ODFs trained from meshes have significantly lower chamfer error than point clouds reconstructed using ODFs trained from depth maps. This is because input mesh representation provides more flexibility in sampling ray start points and directions (different for each sampled ray) compared to the ODF training data sampled from depth maps (ray start point same for all rays of one depth map). This can be fixed at the cost of sampling more multi-view depth maps.

7 Conclusion

In this paper, we introduced a new 3D shape representation that we call Omnidirectional Distance Fields (ODFs). ODFs represent shape by encoding the distance and visibility of rays originating at any 3D location and pointed in any direction. Because of the omnidirectional information, ODFs make it more efficient to transform between different representations using forward maps. Since ODFs are high dimensional and expensive, we use a neural network, NeuralODF to learn the ODF implicitly. We show that an MLP architecture can effectively learn an ODF and can be used to query the ODF continuously at arbitrary resolutions. Results show that we can capture high-quality shapes with NeuralODF and can efficiently forward map to common 3D representations like point clouds, depth images, meshes and voxel grids.

Limitations: Our method has several limitations which we plan to address in future work. First, ODFs are high dimensional fields that are harder to learn than standard SDFs or UDFs, yet we show that a standard MLP can learn it with a recursive strategy. Our Jumping Cubes algorithm works reliably for close shapes but can sometimes have trouble with open surfaces since it does not know which holes are spurious. NeuralODF does not beat other methods in shape representation quality, but our goal is present it as an alternative option.

Societal Impacts: AI systems that use NeuralODF for shape representation can suffer from bias introduced by the dataset we use. More diverse shapes will have to be introduced to avoid such biases. Training NeuralODF uses several GPU-days of compute that results in energy consumption. Future work should investigate mitigating the large energy usage.

References

- [1] Panos Achlioptas, Olga Diamanti, Ioannis Mitliagkas, and Leonidas Guibas. Learning representations and generative models for 3d point clouds. In *International conference on machine learning*, pages 40–49. PMLR, 2018.
- [2] Tristan Aumentado-Armstrong, Stavros Tsogkas, Sven Dickinson, and Allan Jepson. Representing 3d shapes with probabilistic directed distance fields. *IEEE/CVF Conference on Computer Vision and Pattern Recognition (CVPR)*, 2022.
- [3] Jimmy Lei Ba, Jamie Ryan Kiros, and Geoffrey E. Hinton. Layer normalization, 2016.
- [4] James R Bergen and Edward H Adelson. The plenoptic function and the elements of early vision. *Computational models of visual processing*, 1:8, 1991.
- [5] Fausto Bernardini, Joshua Mittleman, Holly Rushmeier, Cláudio Silva, and Gabriel Taubin. The ball-pivoting algorithm for surface reconstruction. *IEEE transactions on visualization and computer graphics*, 5(4):349–359, 1999.
- [6] Bharat Lal Bhatnagar, Garvita Tiwari, Christian Theobalt, and Gerard Pons-Moll. Multi-garment net: Learning to dress 3d people from images. In *Proceedings of the IEEE/CVF international conference on computer vision*, pages 5420–5430, 2019.
- [7] Michael M Bronstein, Joan Bruna, Yann LeCun, Arthur Szlam, and Pierre Vandergheynst. Geometric deep learning: going beyond euclidean data. *IEEE Signal Processing Magazine*, 34(4):18–42, 2017.
- [8] Angel X Chang, Thomas Funkhouser, Leonidas Guibas, Pat Hanrahan, Qixing Huang, Zimo Li, Silvio Savarese, Manolis Savva, Shuran Song, Hao Su, et al. Shapenet: An information-rich 3d model repository. *arXiv preprint arXiv:1512.03012*, 2015.
- [9] Zhiqin Chen and Hao Zhang. Learning implicit fields for generative shape modeling. In *Proceedings of the IEEE/CVF Conference on Computer Vision and Pattern Recognition*, pages 5939–5948, 2019.
- [10] Julian Chibane, Gerard Pons-Moll, et al. Neural unsigned distance fields for implicit function learning. *Advances in Neural Processing Systems*, 33:21638–21652, 2020.

- [11] Christopher B Choy, Danfei Xu, JunYoung Gwak, Kevin Chen, and Silvio Savarese. 3d-r2n2: A unified approach for single and multi-view 3d object reconstruction. In *European conference on computer vision*, pages 628–644. Springer, 2016.
- [12] Brian Curless and Marc Levoy. A volumetric method for building complex models from range images. In *Proceedings of the 23rd Annual Conference on Computer Graphics and Interactive Techniques, SIGGRAPH '96*, page 303–312, New York, NY, USA, 1996. Association for Computing Machinery.
- [13] Angela Dai and Matthias Nießner. Scan2mesh: From unstructured range scans to 3d meshes. In *Proceedings of the IEEE/CVF Conference on Computer Vision and Pattern Recognition*, pages 5574–5583, 2019.
- [14] Theo Deprelle, Thibault Groueix, Matthew Fisher, Vladimir Kim, Bryan Russell, and Mathieu Aubry. Learning elementary structures for 3d shape generation and matching. *Advances in Neural Network Processing Systems*, 32, 2019.
- [15] Yueqi Duan, Haidong Zhu, He Wang, Li Yi, Ram Nevatia, and Leonidas J Guibas. Curriculum deepsf. In *European Conference on Computer Vision*, pages 51–67. Springer, 2020.
- [16] Matheus Gadelha, Rui Wang, and Subhransu Maji. Multiresolution tree networks for 3d point cloud processing. In *Proceedings of the European Conference on Computer Vision (ECCV)*, pages 103–118, 2018.
- [17] Georgia Gkioxari, Jitendra Malik, and Justin Johnson. Mesh r-cnn. In *Proceedings of the IEEE/CVF International Conference on Computer Vision*, pages 9785–9795, 2019.
- [18] Steven Gortler, Radek Grzeszczuk, Richard Szeliski, and Michael Cohen. The lumigraph. *Proc. of SIGGRAPH 96*, 96, 08 2001.
- [19] Amos Gropp, Lior Yariv, Niv Haim, Matan Atzmon, and Yaron Lipman. Implicit geometric regularization for learning shapes. *arXiv preprint arXiv:2002.10099*, 2020.
- [20] Amos Gropp, Lior Yariv, Niv Haim, Matan Atzmon, and Yaron Lipman. Implicit geometric regularization for learning shapes. In *Proceedings of Machine Learning and Systems 2020*, pages 3569–3579. 2020.
- [21] Thibault Groueix, Matthew Fisher, Vladimir G Kim, Bryan C Russell, and Mathieu Aubry. A papier-mâché approach to learning 3d surface generation. In *Proceedings of the IEEE conference on computer vision and pattern recognition*, pages 216–224, 2018.
- [22] Kan Guo, Dongqing Zou, and Xiaowu Chen. 3d mesh labeling via deep convolutional neural networks. *ACM Transactions on Graphics (TOG)*, 35(1):1–12, 2015.
- [23] Rana Hanocka, Amir Hertz, Noa Fish, Raja Giryes, Shachar Fleishman, and Daniel Cohen-Or. Meshcnn: a network with an edge. *ACM Transactions on Graphics (TOG)*, 38(4):1–12, 2019.
- [24] John C Hart. Sphere tracing: A geometric method for the antialiased ray tracing of implicit surfaces. *The Visual Computer*, 12(10):527–545, 1996.
- [25] Alec Jacobson. <https://github.com/alecjacobson/common-3d-test-models>.
- [26] Danilo Jimenez Rezende, SM Eslami, Shakir Mohamed, Peter Battaglia, Max Jaderberg, and Nicolas Heess. Unsupervised learning of 3d structure from images. *Advances in neural network processing systems*, 29, 2016.
- [27] Michael Kazhdan, Matthew Bolitho, and Hugues Hoppe. Poisson surface reconstruction. In *Proceedings of the fourth Eurographics symposium on Geometry processing*, volume 7, 2006.
- [28] Michael Landy and J. Anthony Movshon. *The Plenoptic Function and the Elements of Early Vision*, pages 3–20. 1991.
- [29] Jiahui Lei, Srinath Sridhar, Paul Guerrero, Minhyuk Sung, Niloy Mitra, and Leonidas J Guibas. Pix2surf: Learning parametric 3d surface models of objects from images. In *European Conference on Computer Vision*, pages 121–138. Springer, 2020.
- [30] Marc Levoy and Pat Hanrahan. Light field rendering. In *Proceedings of the 23rd Annual Conference on Computer Graphics and Interactive Techniques, SIGGRAPH '96*, page 31–42, New York, NY, USA, 1996. Association for Computing Machinery.
- [31] Chun-Liang Li, Manzil Zaheer, Yang Zhang, Barnabas Poczos, and Ruslan Salakhutdinov. Point cloud gan. *arXiv preprint arXiv:1810.05795*, 2018.
- [32] Yiyi Liao, Simon Donne, and Andreas Geiger. Deep marching cubes: Learning explicit surface representations. In *Proceedings of the IEEE Conference on Computer Vision and Pattern Recognition*, pages 2916–2925, 2018.
- [33] Fayao Liu, Chunhua Shen, and Guosheng Lin. Deep convolutional neural fields for depth estimation from a single image. In *Proceedings of the IEEE conference on computer vision and pattern recognition*, pages 5162–5170, 2015.
- [34] William E Lorensen and Harvey E Cline. Marching cubes: A high resolution 3d surface construction algorithm. *ACM siggraph computer graphics*, 21(4):163–169, 1987.
- [35] Lars Mescheder, Michael Oechsle, Michael Niemeyer, Sebastian Nowozin, and Andreas Geiger. Occupancy networks: Learning 3d reconstruction in function space. In *Proceedings of the IEEE/CVF Conference on Computer Vision and Pattern Recognition*, pages 4460–4470, 2019.
- [36] Ben Mildenhall, Pratul P Srinivasan, Matthew Tancik, Jonathan T Barron, Ravi Ramamoorthi, and Ren Ng. Nerf: Representing scenes as neural radiance fields for view synthesis. In *European conference on computer vision*, pages 405–421. Springer, 2020.
- [37] Paritosh Mittal, Yen-Chi Cheng, Maneesh Singh, and Shubham Tulsiani. Autosdf: Shape priors for 3d completion, reconstruction and generation. *arXiv preprint arXiv:2203.09516*, 2022.
- [38] Jeong Joon Park, Peter Florence, Julian Straub, Richard Newcombe, and Steven Lovegrove. Deepsf: Learning continuous signed distance functions for shape representation. In *Proceedings of the IEEE/CVF*

- Conference on Computer Vision and Pattern Recognition*, pages 165–174, 2019.
- [39] Songyou Peng, Michael Niemeyer, Lars Mescheder, Marc Pollefeys, and Andreas Geiger. Convolutional occupancy networks. In *European Conference on Computer Vision*, pages 523–540. Springer, 2020.
- [40] Ken Perlin and Eric M Hoffert. Hypertexture. In *Proceedings of the 16th annual conference on Computer graphics and interactive techniques*, pages 253–262, 1989.
- [41] Charles R Qi, Hao Su, Kaichun Mo, and Leonidas J Guibas. Pointnet: Deep learning on point sets for 3d classification and segmentation. In *Proceedings of the IEEE conference on computer vision and pattern recognition*, pages 652–660, 2017.
- [42] Charles Ruizhongtai Qi, Li Yi, Hao Su, and Leonidas J Guibas. Pointnet++: Deep hierarchical feature learning on point sets in a metric space. *Advances in neural network processing systems*, 30, 2017.
- [43] Franco Scarselli and Ah Chung Tsoi. Universal approximation using feedforward neural networks: A survey of some existing methods, and some new results. *Neural networks*, 11(1):15–37, 1998.
- [44] Matan Shoef, Sharon Fogel, and Daniel Cohen-Or. Pointwise: An unsupervised point-wise feature learning network. *arXiv preprint arXiv:1901.04544*, 2019.
- [45] Vincent Sitzmann, Semon Rezchikov, Bill Freeman, Josh Tenenbaum, and Fredo Durand. Light field networks: Neural scene representations with single-evaluation rendering. *Advances in Neural Network Processing Systems*, 34, 2021.
- [46] Vincent Sitzmann, Michael Zollhöfer, and Gordon Wetzstein. Scene representation networks: Continuous 3d-structure-aware neural scene representations. *Advances in Neural Network Processing Systems*, 32, 2019.
- [47] Vincent Sitzmann, Michael Zollhöfer, and Gordon Wetzstein. Scene representation networks: Continuous 3d-structure-aware neural scene representations. In *Advances in Neural Network Processing Systems*, 2019.
- [48] Nanyang Wang, Yinda Zhang, Zhuwen Li, Yanwei Fu, Wei Liu, and Yu-Gang Jiang. Pixel2mesh: Generating 3d mesh models from single rgb images. In *Proceedings of the European conference on computer vision (ECCV)*, pages 52–67, 2018.
- [49] Peng Wang, Lingjie Liu, Yuan Liu, Christian Theobalt, Taku Komura, and Wenping Wang. Neus: Learning neural implicit surfaces by volume rendering for multi-view reconstruction. *arXiv preprint arXiv:2106.10689*, 2021.
- [50] Yue Wang, Yongbin Sun, Ziwei Liu, Sanjay E Sarma, Michael M Bronstein, and Justin M Solomon. Dynamic graph cnn for learning on point clouds. *Acm Transactions On Graphics (tog)*, 38(5):1–12, 2019.
- [51] Ruben Wiersma, Elmar Eisemann, and Klaus Hildebrandt. Cnns on surfaces using rotation-equivariant features. *ACM Transactions on Graphics (TOG)*, 39(4):92–1, 2020.
- [52] Yiheng Xie, Towaki Takikawa, Shunsuke Saito, Or Litany, Shiqin Yan, Numair Khan, Federico Tombari, James Tompkin, Vincent Sitzmann, and Srinath Sridhar. Neural fields in visual computing and beyond. *Computer Graphics Forum*, 2022.
- [53] Xingguang Yan, Liqiang Lin, Niloy J Mitra, Dani Lischinski, Danny Cohen-Or, and Hui Huang. Shapeformer: Transformer-based shape completion via sparse representation. *arXiv preprint arXiv:2201.10326*, 2022.
- [54] Guandao Yang, Xun Huang, Zekun Hao, Ming-Yu Liu, Serge Belongie, and Bharath Hariharan. Pointflow: 3d point cloud generation with continuous normalizing flows. In *Proceedings of the IEEE/CVF International Conference on Computer Vision*, pages 4541–4550, 2019.
- [55] Yaoqing Yang, Chen Feng, Yiru Shen, and Dong Tian. Foldingnet: Point cloud auto-encoder via deep grid deformation. In *Proceedings of the IEEE conference on computer vision and pattern recognition*, pages 206–215, 2018.
- [56] Zhangsiahao Yang, Or Litany, Tolga Birdal, Srinath Sridhar, and Leonidas Guibas. Continuous geodesic convolutions for learning on 3d shapes. In *Proceedings of the IEEE/CVF Winter Conference on Applications of Computer Vision*, pages 134–144, 2021.
- [57] Lior Yariv, Jiatao Gu, Yoni Kasten, and Yaron Lipman. Volume rendering of neural implicit surfaces. *Advances in Neural Network Processing Systems*, 34, 2021.
- [58] Jianglong Ye, Yuntao Chen, Naiyan Wang, and Xiaolong Wang. Gifs: Neural implicit function for general shape representation. *arXiv preprint arXiv:2204.07126*, 2022.
- [59] Matthias Zwicker, Hanspeter Pfister, Jeroen Van Baar, and Markus Gross. Surface splatting. In *Proceedings of the 28th annual conference on Computer graphics and interactive techniques*, pages 371–378, 2001.

8 Abstract

In this supplementary material, we first showcase the training procedure and results when the NeuralODF was trained with depth images as the input representation (depth images \rightarrow ODF \rightarrow point cloud). Next, we describe in detail the core Jumping Cubes and the recursive marching algorithms. Finally, we showcase additional generalization results of NeuralODF on the Shapenet categories.

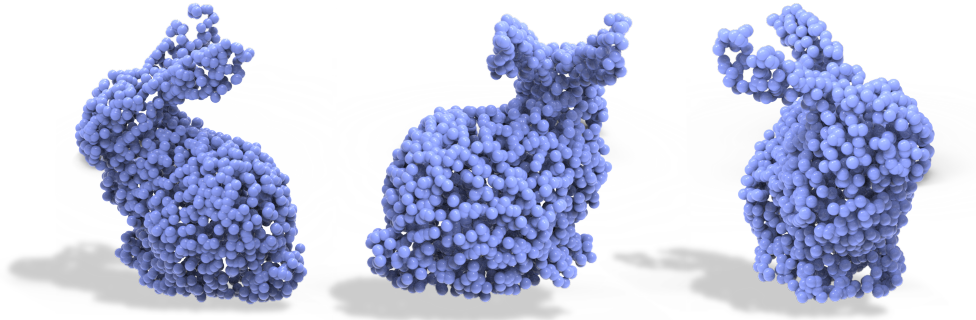


Figure 7: Point cloud reconstructions of the Stanford Bunny, retrieved from a NeuralODF trained on 32 depth images.

9 Training with depth images

The results shown for our overfitting and generalization experiments with NeuralODF were trained using mesh data. However, since the basic input of NeuralODF is a ray, we are also able to train on multi-view depth images and point clouds with normals. The details for how training data is generated from these representations is in the Training Data Preparation section of the paper. While point clouds with normals allow us to sample rays in a manner similar to meshes, depth images give us a ray bundle that provides a more biased sampling of our input domain. In Figure 7 we show a pointcloud reconstruction obtained from a NeuralODF trained on 32 depth images from cameras sampled uniformly from a sphere around the Stanford Bunny. These results show that we are still able to accurately learn an ODF when using depth images instead of a more complete representation such as a point cloud or a mesh.

10 Jumping Cubes

10.1 Mesh extraction on open surfaces

The Marching Cubes algorithm is commonly used to extract a mesh surface from implicit functions. It achieves this by evaluating the implicit function at the vertices of a 3D lattice grid. Each cube within the lattice can then be triangulated according to the sign of the function at each corner of the cube. As NeuralODF is an unsigned representation, this technique is not possible for us. However, by predicting surface depth, we can estimate which cube edge will intersect the object surface. An edge is determined to be intersected when the predicted depth at the vertex at one end of the edge is less than the length of the edge itself. Then, we can triangulate each cube based on which of its 12 edges are intersected by the object surface. The Marching Cubes algorithm has 2^8 cases which can be reduced down to 14 base cases by removing configurations that are equivalent up to some rotation or change of sign. Similarly, for Jumping Cubes, we find that there are 2^{12} cases which can be reduced down to 218 cases when we account for rotations. In order to find the correct triangulation for each cube and produce a mesh, Jumping Cubes requires a binary array that indicates whether the surface intersects each cube edge on a 3 dimensional lattice grid. After extracting the surface with Jumping Cubes we run Laplacian smoothing.

10.2 Efficient jumping cubes with NeuralODF

By predicting surface depth, ODFs allow us to efficiently compute the intersection array necessary to apply Jumping Cubes. In an $n \times n \times n$ lattice grid, there are $3n^3$ cube edges, or n^3 edges for each axis. On one side of the lattice grid, there are n^2 points, each positioned at the head of a column of n cube edges. For each of these columns, we use Algorithm 1 to efficiently compute the depth value for each vertex in the column. The number of ODF queries this algorithm makes is dependent on the number of object surfaces the column passes through, not on the resolution of the grid. Therefore, we can run Jumping Cubes with only $\mathcal{O}(n^2)$ network queries, whereas Marching Cubes requires $\mathcal{O}(n^3)$

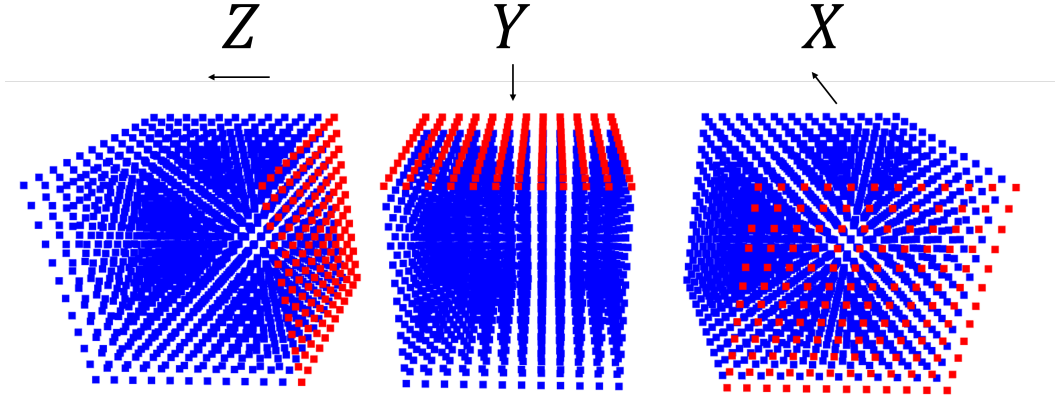


Figure 8: For Jumping Cubes, we must evaluate the depth at each lattice point, for each of the 3 axis-aligned viewing directions. Instead of directly querying each point, we start at the red points and jump down the column of points according to the predicted depth.

network queries.

Algorithm 1 ODF single-column inference for jumping cubes

```

1:  $x \leftarrow$  Starting position
2:  $\hat{w} \leftarrow$  Viewing direction
3:  $b \leftarrow$  Steps adjustment
4:  $s \leftarrow$  Distance between vertices in the grid
5:
6: AllDepths = []
7: while Not at end of column do
8:   depth, intersection =  $f(x, \hat{w})$ 
9:   if no intersection then
10:    set depth to a default value (0.5)
11:   steps  $\leftarrow \max(1, \lfloor \frac{\text{depth}}{s} - b \rfloor)$ 
12:   AllDepths += [depth +  $\hat{w} \cdot s \cdot 0$ ), ..., depth +  $\hat{w} \cdot s \cdot (\text{steps}-1)$ ]
13:    $x \leftarrow x + \hat{w} \cdot s \cdot \text{steps}$ 
return AllDepths

```

11 Recursive inference

In this section, we discuss the details of the recursive inference. Firstly, given a starting position x and viewing direction \hat{w} , we clamp the predicted depth d since the depth larger than the clamping value ψ is not constrained by the loss function (see algorithm 2 and 3 line 1-7). Secondly, we run the inference $n - 1$ times. For each iteration, we check the forward and backward direction inference except for the first iteration and pick the minimum one to prevent overshooting the point x (see algorithm 3 line 8-17). Finally, an additional forward and backward direction inference is used to generate the mask from the depth branch (see algorithm 3 line 18-22).

12 Ablation study of data augmentation

The recursive property of ODFs enables efficient data usage through dataset augmentation. Table 6 shows that learning an ODF without using any data augmentations is a challenging task. However, utilizing the recursive property efficiently through dataset augmentation can greatly improve the quality of our NeuralODF. The Table 6 results also show that using Aug-a alone results in significantly

Algorithm 2 An inference

```
1:  $x \leftarrow$  Starting position
2:  $\hat{w} \leftarrow$  Viewing direction
3:  $\psi \leftarrow$  Clamping value
4:  $d, m = f(x, \hat{w})$ 
5: return  $\min(d, \psi), m$ 
```

Algorithm 3 Recursive Inference for Neural ODF

```
1:  $x \leftarrow$  Starting position
2:  $\hat{w} \leftarrow$  Viewing direction
3:  $n \leftarrow$  Number of recursive calls
4:  $\tau \leftarrow$  Surface margin
5: Get forward direction inference by Algorithm 2
6:  $x \leftarrow x + d_{\text{forward}} \cdot \hat{w}$ 
7:  $m \leftarrow m_{\text{forward}}$ 
8:  $n \leftarrow n - 1$ 
9: while  $n \neq 0$  do
10: Get forward and backward direction inference by Algorithm 2
11:   if  $d_{\text{forward}} \leq d_{\text{backward}}$  then
12:      $x \leftarrow x + d_{\text{forward}} \cdot \hat{w}$ 
13:      $m \leftarrow m_{\text{forward}}$ 
14:   else
15:      $x \leftarrow x + d_{\text{backward}} \cdot -\hat{w}$ 
16:      $m \leftarrow m_{\text{backward}}$ 
17:    $n \leftarrow n - 1$ 
18: Get forward and backward direction inference by Algorithm 2
19: if  $d_{\text{forward}} \leq d_{\text{backward}}$  then
20:    $m \leftarrow m \cap d_{\text{forward}} < \tau$ 
21: else
22:    $m \leftarrow m \cap d_{\text{backward}} < \tau$ 
return  $x, m$ 
```

better quality than using Aug-b or Aug-c alone. We hypothesize that this may arise from the fact that Aug-b and Aug-c may include some error in the depth labels when non-target surfaces appear within the augmentation margin. Nevertheless, enabling all three augmentation strategies still yields the best reconstruction and improves the Chamfer Distance by 0.175 over the Aug-a only model.

Aug-a	Aug-b	Aug-c	CD \downarrow	Rec. (%) \uparrow	F-score (%) \uparrow
			5.5614	44.05	58.62
✓			0.4775	90.60	92.87
	✓		0.8383	87.29	84.95
		✓	0.8460	89.61	85.34
✓	✓	✓	0.3025	96.29	94.65

Table 6: Ablation Study for dataset augmentation. See Section 5.1 for the details.

13 Additional Results

In our generalization experiments, we used an autodecoder framework to train NeuralODF to represent object classes. Here we show reconstructions of additional instances from from these classes. Each instance shown here was not present in the training data, but was fit to the trained model by optimizing a latent code.

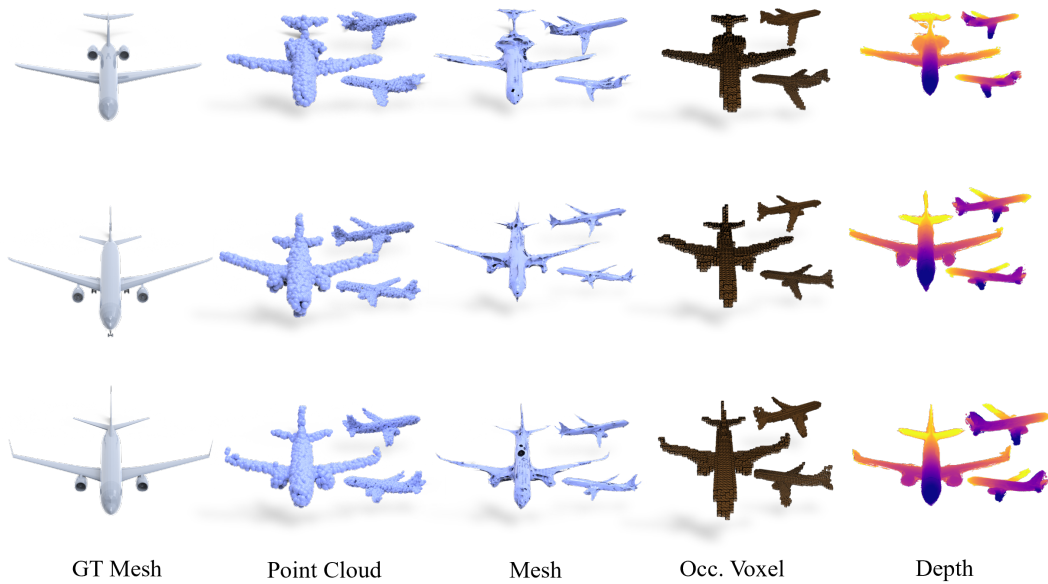


Figure 9: Reconstruction of unseen instances of the Shapenet airplanes class.

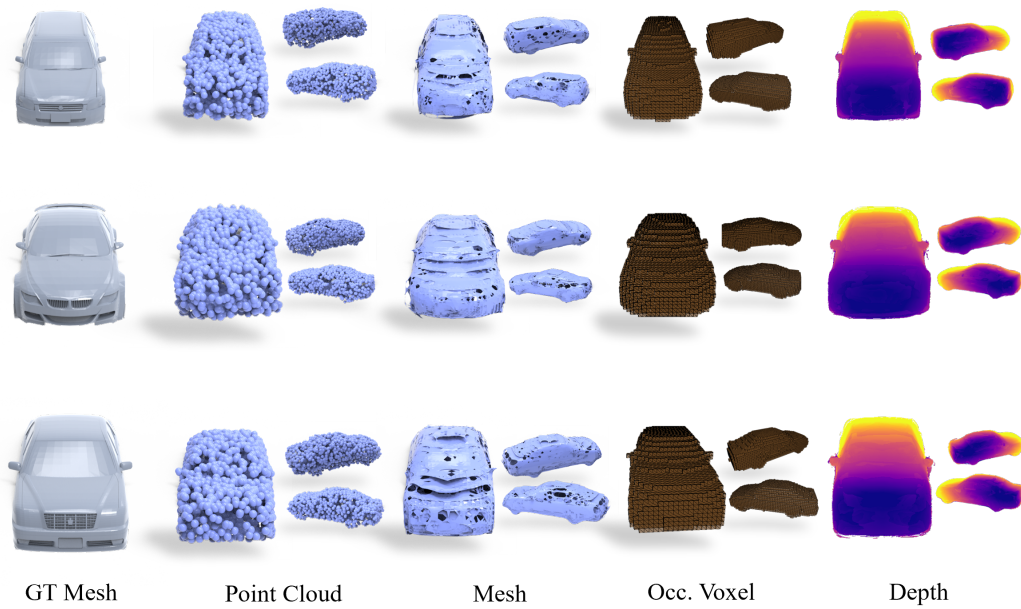


Figure 10: Reconstruction of unseen instances of the Shapenet cars class.

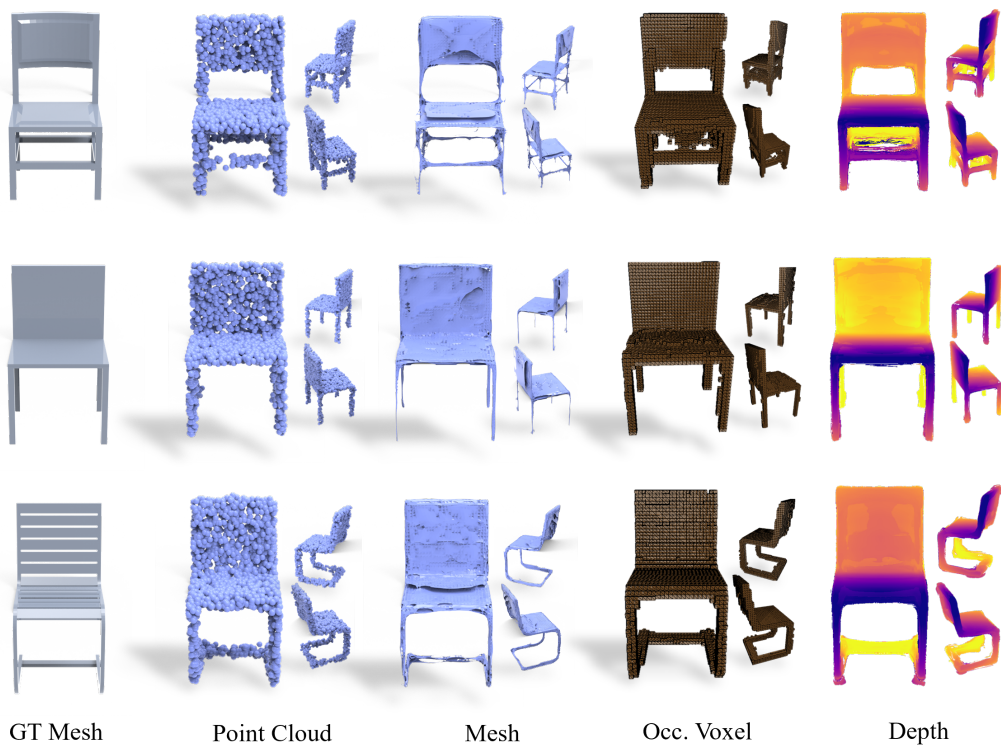


Figure 11: Reconstruction of unseen instances of the Shapenet chairs class.